

Photocurrent dynamics in a poly(phenylene vinylene)-based photorefractive compositeL. Kulikovskiy,¹ D. Neher,^{1,*} E. Mecher,² K. Meerholz,² H.-H. Hörhold,³ and O. Ostroverkhova⁴¹University of Potsdam, Institute for Physics, Am Neuen Palais 10, 14469 Potsdam, Germany²Department of Physical Chemistry, University of Köln, Luxemburgerstrasse 116, 50939 Köln, Germany³Friedrich-Schiller-Universität, Institute for Organic Chemistry and Macromolecular Chemistry, Humboldtstraße 10, 07743 Jena, Germany⁴Department of Physics, University of Alberta, Edmonton, Alberta T6G 2J1, Canada

(Received 23 June 2003; revised manuscript received 4 December 2003; published 25 March 2004)

All parameters describing the charge carrier dynamics in a poly(phenylene vinylene)-based photorefractive (PR) composite relevant to PR grating dynamics were determined using photoconductivity studies under various illumination conditions. In particular, the values of the coefficients for trap filling and recombination of charges with ionized sensitizer molecules could be extracted independently. It is concluded that the PR growth time without preillumination is mostly determined by the competition between deep trap filling and recombination with ionized sensitizer molecules. Further, the pronounced increase in PR speed upon homogeneous preillumination (gating) as reported recently is quantitatively explained by deep trap filling.

DOI: 10.1103/PhysRevB.69.125216

PACS number(s): 71.20.Rv, 42.65.Hw, 42.70.Nq, 72.80.Le

I. INTRODUCTION

The photorefractive (PR) effect is the spatial variation of the refractive index in an electrooptically active material in response to the formation a space-charge field in a photoconductor upon nonuniform illumination with light. This effect involves several photophysical processes: (a) the photogeneration of charge carriers, (b) transport and trapping of these charges, resulting in the buildup of a space charge field, and (c) creation of a refractive index contrast due to electrooptical (EO) effects. Because these processes are fully reversible, PR materials have been intensively studied with respect to their application in holography, data storage and time-gated holographic imaging (TGHI).¹⁻⁴ While the PR effect in inorganic crystals has been known for 30 years, the first polymer exhibiting PR properties was reported in 1991.⁵ Since then, the efficiency of PR composites based on polymeric or glassy-organic materials has been considerably improved, reaching values of close to 100%.⁶⁻¹¹ In order to exhibit the PR effect, these materials must contain different functional moieties, providing photosensitivity, charge transport, and electrooptical properties. Most of the organic PR composites reported by now consist of low molecular weight charge-transporting moieties covalently attached to a passive polymeric backbone such as in polyvinylcarbazole (PVK) or polysiloxanes.^{6,9} Alternatively, photorefractive molecular glasses have been reported, which combine the charge-transporting moiety and the electrooptically active unit in one molecule.¹²⁻¹⁴ More recently, main chain conjugated polymers have been introduced as fast and efficient PR materials.¹⁵⁻¹⁸

However, until recently, no PR materials exhibited a large PR response combined with a fast response in the near infrared, a wavelength range particularly attractive for the investigation of biological samples with TGHI. In a recent work, Mecher *et al.* demonstrated a near-infrared-sensitive PR polymer composite based on a photoconductive poly(phenylene-vinylene) copolymer (TPD-PPV),¹⁹ sensitized with the highly soluble fullerene derivative (PCBM).¹⁸

When the two writing beams (wavelength 830 nm, total external write-beam intensity 3.27 W/cm²) in the four-wave mixing experiment were switched on simultaneously, the material exhibited a rather slow response with grating build-up times in the range of seconds. If, however, the sample was homogeneously preilluminated at 633 nm with a pulse of approximately 1 s length and a light intensity of 5.2 W/cm², an almost 40× improvement in recording speed was observed. This effect was explained by the creation of a uniform distribution of mobile charge carriers (in this case holes) upon preillumination, which is spatially modulated by the intensity pattern of the two interfering writing beams.

In this paper we provide the quantitative understanding of the processes governing the build-up of the space charge field, either without or with preillumination. We present a detailed study of the parameters describing trapping, detrapping and recombination in this PR composite. It is shown that without preillumination, the temporal evolution of the space charge field is mainly governed by the filling of deep traps, in competition with the recombination of the photogenerated charges with ionized sensitizer molecules. Our results further show that the improvements in PR speed upon preillumination are mainly caused by the filling of these traps, resulting in a large and homogenous density of ionized sensitizer molecules.

II. THEORY

While the large diffraction efficiencies observed in several PR composites can be well understood by the orientation of chromophores with a large anisotropy of the molecular polarizability by the space charge field (the so-called orientational enhancement effect),^{6,8,10,20} the factors controlling the PR response time are discussed controversially.²¹⁻²⁵ Both, the theory by Kukhtarev,²⁶ originally developed to describe the PR response in inorganic materials, as well as Schildkraut's model for organic PR composites^{27,28} have been used in an attempt to correlate photophysical parameters and characteristic PR growth times.^{23,29-31} The latter model involves

several basic photophysical steps such as the photogeneration of free charge carriers on the photoconductive host via photoionization of sensitizer molecules, the drift of these charges and trapping into neutral traps, and finally detrapping from these traps and recombination with ionized sensitizer molecules. The kinetics of these processes is governed by various parameters such as the total density of traps and the coefficients for carrier trapping, thermal detrapping, and recombination. Therefore, the complete understanding of the response of a PR composite requires knowledge of all of these quantities.

In a recent paper, Ostroverkhova and Singer have studied the photocurrent dynamics and the PR growth characteristics of various PVK-based PR materials.²⁵ They were able to correlate the characteristic rise times of single-pulse transient photocurrent experiments to the values of various photophysical parameters relevant to the PR growth. Further, the agreement between experimental PR growth times and model predictions could be substantially improved by introducing a second trapping level into Schildkraut's theory. As outlined in the following, this model is also appropriate to describe the charge carrier kinetics in the TPD-PPV-based composite studied here.

Assuming that the absorption of the material is quite low, the beam intensity can be considered to be constant throughout the whole layer thickness. If one, further, assumes that the sensitizer acts as a deep electron trap, the photocurrent is solely determined by the motion of holes in the polymer matrix. Then, the transient photoconductivity can be described by the following set of equations:

$$j_{\text{photo}}(t) = e\rho(t)\mu E, \quad (1a)$$

$$\rho(t) = S^-(t) - T^+(t) - M^+(t), \quad (1b)$$

$$\frac{\partial S^-(t)}{\partial t} = sI(t)[S - S^-(t)] - \gamma_R\rho(t)S^-(t), \quad (2a)$$

$$\frac{\partial T^+(t)}{\partial t} = \gamma_T\rho(t)[T - T^+(t)] - \beta_T T^+(t), \quad (2b)$$

$$\frac{\partial M^+(t)}{\partial t} = \gamma_M\rho(t)[M - M^+(t)] - \beta_M M^+(t). \quad (2c)$$

Here, ρ is the density of mobile holes, I the light intensity, e the elementary charge, μ the mobility of free holes, E the applied electric field, S the initial density of sensitizer molecules, S^- the density of ionized sensitizers, T^+ and T the densities of filled shallow traps and the total densities of shallow traps, respectively, M^+ and M the densities of filled deep traps and the total densities of deep traps, respectively, γ_T and γ_M the trapping coefficients for shallow and deep traps, β_T and β_M the corresponding thermal detrapping rates, and γ_R the recombination coefficient. Further, the factor s describing photogeneration is given by $s = \phi\alpha\lambda/hcS$ (in the limit of low absorption), with ϕ the quantum efficiency of photogeneration, α the absorption coefficient, λ the wavelength of light, and c the speed of light in vacuum. Note that

equation 1 b implies charge neutrality. All variables and parameters are assumed to be constant throughout the whole layer thickness.

In the work by Ostroverkhova and Singer,²⁵ the generation efficiency ϕ and the carrier mobility μ were measured as a function of electric field using xerographic discharge and time-of-flight experiments. Further, the values of the parameters γ_R , β_T , β_M , $\gamma_T \times T$, and $\gamma_M \times M$ were determined from the analysis of the characteristic growth times of single pulse transient photoconductivity experiments. However, their analysis did not allow for an independent determination of trap densities and trapping coefficients.

In the following, we demonstrate that all parameters describing trapping and recombination can be determined experimentally using single-pulse, double-pulse, and cw-photoconductivity experiments. Further, these parameters are used to simulate the growth of the space charge field under the experimental conditions as reported in Ref. 18.

III. EXPERIMENTAL

The photorefractive composite studied here is based on a photoconductive poly(phenylene-vinylene) copolymer (TPD-PPV) (Ref. 19) (56 wt. %), an eutectic mixture of two azobenzene EO chromophores [2,5-dimethyl-(4-p-nitrophenylazo)-anisole and 3-methoxy-(4-p-nitrophyslazo)-anisole, wt. ratio 1:1, 30 wt. % total concentration], the plasticizer diphenyl-phthalate (13 wt. %) and a highly soluble fullerene derivative (PCBM, 1 wt. %) as the sensitizer.¹⁸ The resulting composite has a glass transition temperature T_g of 10 °C. For this composition, a sensitizer density S of $8 \times 10^{18} \text{ cm}^{-3}$ was calculated.

For our studies, the material was sandwiched between two ITO-coated glass substrates, yielding a thickness of the active layer of 37 μm . All photoconductivity experiments were performed at room temperature by illumination with a diode-laser (spot size around 0.04 cm^2) operating at a wavelength of 690 nm and an intensity of 5–200 mW/cm^2 . At this wavelength the absorption coefficient α is 50 cm^{-1} , which allowed us to perform fast transient photocurrent measurements at moderate intensities with homogeneous light intensity throughout the active layer. Note that the PR experiments published in Ref. 18 had been performed with a writing wavelength of 830 nm and a gating wavelength of 633 nm.

A constant electric field of up to 27 $\text{V}/\mu\text{m}$ was applied around 60 s before starting the transient photocurrent experiments. Under these conditions the dark current was around $0.5 \times 10^{-6} \text{ A}/\text{cm}^2$, well below the typical photocurrents. The light pulses were formed by an electro-optical modulator (LM0202P from Linos) controlled by a pulse generator (Agilent 33120A). The time evolution of the photocurrent was measured with a digital storage oscilloscope (Tektronix 210) using a photocurrent multiplier (P9202-4 from Gigahertz-Optik). The electric field was applied with a source-measure unit (Keithley 237), which also served as the electrometer in the dc-photoconductivity experiments. Xerographic discharge experiments have been performed to deter-

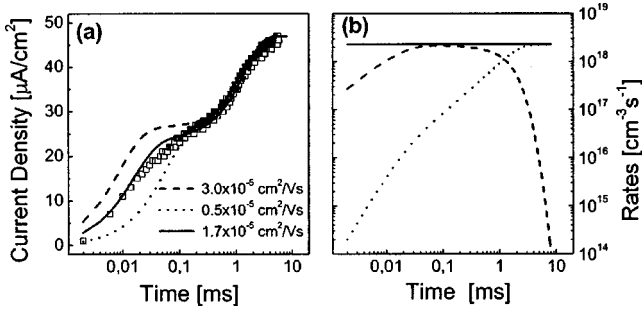


FIG. 1. (a) Experimental photocurrent transients (open squares) with single pulse illumination, measured at an intensity of 100 mW cm^{-2} and an electric field of $25 \text{ V } \mu\text{m}^{-1}$. Also shown are the results of numerical simulations with Eqs. (1) and (2) (lines), assuming three different hole mobilities. All other parameters were varied to give the best agreement to the experimental data. Further, deep trap filling was neglected by setting, $M=0$. (b) The rates $d\rho/dt$ for carrier generation (solid line), trapping (dashed line) and recombination (dotted line) according to Eqs. (1) and (2), for the simulation with a mobility of $\mu=1.7 \times 10^{-5} \text{ cm}^2 \text{ V}^{-1} \text{ s}^{-1}$.

mine the quantum efficiency ϕ as a function of the electric field.³²

IV. RESULTS AND DISCUSSIONS

A. Determination of free carrier mobility and shallow trapping parameters

A typical photocurrent transient for short-pulse illumination is shown in Fig. 1(a). It is characterized by a continuous growth of the photocurrent. As outlined in the following, the photocurrent transients for single pulses of up to 10 ms duration are almost entirely determined by trapping of holes by one trapping species (here denoted as shallow traps) and recombination of the charge carriers with ionized sensitizer molecules.

The experimental transients of the photocurrent density $j_{\text{photo}}(t)$ could be satisfactorily modeled using Eqs. (1) and (2) with setting $M=0$. Interestingly, a good agreement with the experimental results was only possible within a rather narrow range of mobilities, regardless of the choice of all other variable parameters. To illustrate this point, we have simulated the experimental transients with Eqs. (1) and (2), varying all parameters except the mobility. The results are shown in Fig. 1(a) for three different values of μ . Apparently, the initial rise of the photocurrent can be only described by using a mobility in the vicinity of $1.5\text{--}1.9 \times 10^{-5} \text{ cm}^2/\text{V s}$. This large sensitivity of the initial slope to the value of μ is due to the fact that in this early stage of illumination, the density of free holes and thus the rates for carrier trapping and recombination are insignificant [see Fig. 1(b)]. Thus, the initial photocurrent rise is determined by the generation and drift of free carriers, resulting in

$$\frac{dj_{\text{photo}}}{dt} = \mu e E \frac{\phi \alpha \lambda}{hc} I. \quad (3)$$

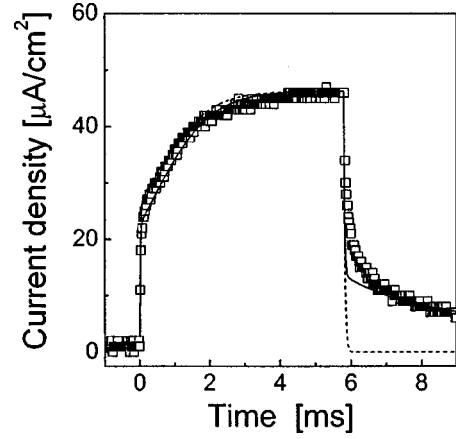


FIG. 2. Photocurrent density measured at $25 \text{ V } \mu\text{m}^{-1}$ and a light intensity of 100 mW cm^{-2} (open squares). Lines show simulations according to Eqs. (1) and (2) assuming only shallow traps ($M=0$) and including detrapping (solid line), or without detrapping ($\beta_T=0$) (dashed line).

With $\phi=0.13$ measured by xerographic experiments at a field of $25 \text{ V}/\mu\text{m}$, the best fit was obtained for a hole mobility of $\mu=1.7 \times 10^{-5} \text{ cm}^2/\text{V s}$.

The further evolution of the photocurrent transient is characterized by two processes associated with two time constants and two plateau values. The analysis of the trapping and recombination rates from the theoretical simulation shows that the first plateau appearing after around 0.1 ms is characterized by the equality of the generation rate and the trapping rate [see Fig. 1(b)], yielding

$$\rho_{P1} \approx \frac{\phi \alpha I}{h \nu \gamma_T T}. \quad (4a)$$

In the second plateau (appearing at the end of the pulse), the density of filled shallow traps T^+ has reached its steady-state value and the generation rate is equal to the recombination rate, resulting in

$$\rho_{P2} \approx \frac{\phi \alpha I}{h \nu \gamma_R T^+}. \quad (4b)$$

If one further presumes that all hole traps are filled at the end of the pulse ($T^+=T$), the ratio between the hole densities in the first and the second plateau and of the corresponding photocurrent densities j_{P1} and j_{P2} (assuming a constant mobility) is proportional to the ratio of the recombination coefficient γ_R and the trapping coefficient γ_T : $j_{P1}/j_{P2} \cong \rho_{P1}/\rho_{P2} = \gamma_R/\gamma_T$. The observation that the photocurrent in the second plateau is larger than in the first plateau suggests that $\gamma_T > \gamma_R$, meaning that the trapping into shallow traps is rapid.

In order to determine the full set of shallow trapping parameters, both the rise and the decay of the photocurrent upon pulsed illumination was recorded. Figure 2 shows the experimental PC transients for a pulse length of around 6 ms and the simulations with either neglect or inclusion of detrapping. Values of γ_R , γ_T , T , and β_T were determined by varying these parameters independently to give the best

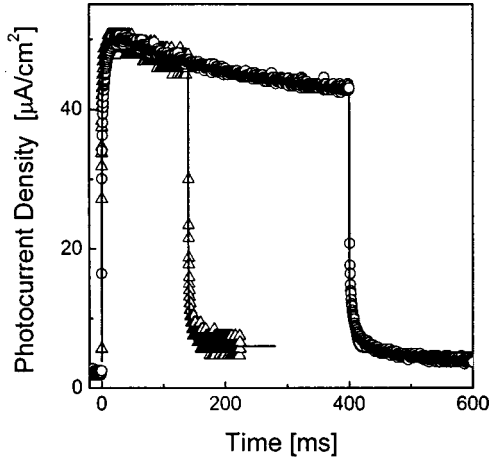


FIG. 3. Photocurrent densities measured at $25 \text{ V } \mu\text{m}^{-1}$ and a light intensity of 100 mW cm^{-2} with a pulse length of 140 ms (open triangles) and 400 ms (open circles). Solid lines show simulations according to Eqs. (1) and (2), taking into account both shallow and deep traps, and using the parameters in Table I.

agreement with the results of single pulse experiments. This procedure yielded $\gamma_R = (1.0 \pm 0.2) \times 10^{-11} \text{ cm}^3 \text{ s}^{-1}$, $\gamma_T = (1.6 \pm 0.4) \times 10^{-11} \text{ cm}^3 \text{ s}^{-1}$, $T = (3.75 \pm 0.5) \times 10^{15} \text{ cm}^{-3}$, and $\beta_T = 300 \pm 125 \text{ s}^{-1}$. Note that the value of γ_R is rather close to a value of $0.85 \times 10^{-11} \text{ cm}^3 \text{ s}^{-1}$ as predicted for Langevin-type recombination (assuming a dielectric constant ϵ of 3.5). Based on the simulations and the shallow trapping parameters, the follow conclusions can be drawn: Under the chosen illumination conditions, the shallow traps are filled within few milliseconds, which is partially due to the exceptionally large trapping coefficient γ_T for shallow traps. Furthermore, the first sharp decay after switching off the light can be attributed to the fast recombination of free charge carriers with ionized sensitizer molecules. The simulation also shows that the following gradual decay of the photocurrent is due to rapid detrapping from shallow traps.

B. Determination of deep trapping parameters

When the sample is illuminated using pulses longer than around 10 ms, a gradual decay of the photocurrent is observed (see, e.g., Fig. 3). Following the line of interpretation in Ref. 25 we attribute this to an increase of the density of recombination centers S^- due to the filling of a second trapping level M (here denoted as deep traps). While the analysis of the photocurrent decay would only yield information on the product $\gamma_M \times M$, it was possible to extract values of M and of the ratio β_M/γ_M independently from the intensity dependence of the photocurrent under cw-illumination.

As can be seen from Eq. (5), which is a simplified version of the steady-state solution of Eqs. (2a)–(2c) for the case $\rho \ll M^+$ (further neglecting shallow trapping and sensitizer depletion), the slope of the intensity dependence of the photocurrent at high intensities is proportional to M^{-1} while the initial sublinear dependence at low intensities as observed experimentally (Fig. 4) can be assigned to detrapping.³³

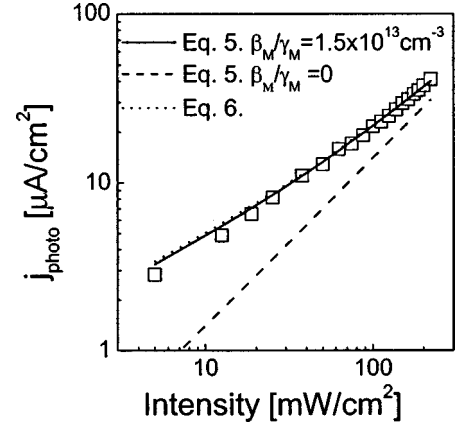


FIG. 4. Dependence of the steady-state photocurrent density j_{photo} (open squares) on the illumination intensity. Also shown are simulations according to Eq. (5), with (solid line) and without thermal detrapping (dashed line) from deep traps. The dotted line shows a simulation according to Eq. (6) taking into account both deep and shallow traps.

$$\rho(I) = \frac{sSI}{2\gamma_RM} \left[1 + \sqrt{1 + \frac{4\gamma_RM\beta_M}{sSI\gamma_M}} \right]. \quad (5)$$

In order to deduce the deep trapping parameters, the experimental intensity dependence was analyzed with the steady-state solution taking into account both trap levels, resulting in a third-order equation for the charge carrier density ρ :

$$a\rho^3 + b\rho^2 - c\rho = d \quad (6a)$$

with

$$a = \gamma_R(M + T),$$

$$b = \left[\gamma_R \left(M \frac{\beta_T}{\gamma_T} + T \frac{\beta_M}{\gamma_M} \right) - \phi \frac{\alpha I}{h\nu} \right],$$

$$c = \phi \frac{\alpha I}{h\nu} \left(\frac{\beta_T}{\gamma_T} + \frac{\beta_M}{\gamma_M} \right),$$

$$d = \phi \frac{\alpha I}{h\nu} \left(\frac{\beta_T}{\gamma_T} \times \frac{\beta_M}{\gamma_M} \right). \quad (6b)$$

Note that Eq. (6) was derived in the limit $\rho \ll M^+$, T^+ , and $M + T \ll S$. According to the values of the photophysical parameters listed in Table I, this approximation is indeed meaningful.

Assuming a constant charge carrier mobility of $1.7 \times 10^{-5} \text{ cm}^2/\text{V s}$ and using values of γ_R , γ_T , T , and β_T as determined from the simulations of short pulse experiments, the best fit to the experimental intensity dependence of the photocurrent yielded $\beta_M/\gamma_M = (1.4 \pm 0.2) \times 10^{13} \text{ cm}^{-3}$ and $M = (1.5 \pm 0.2) \times 10^{16} \text{ cm}^{-3}$. The value of M compares well with typical steady-state densities of ionized sensitizers, measured in PR composites for the case that the EO chromophores do not constitute traps.³⁴ In our PR material, the ionization potential of the used azobenzenes is larger than of

TABLE I. Photoelectric parameters obtained from the comparison of experimental photocurrent data and numerical simulations according to Eqs. (1), (2), and (6).

μ [cm ² /Vs]	γ_R [cm ³ /s]	Shallow traps			Deep traps		
		γ_T [cm ³ /s]	β_T [s ⁻¹]	T [cm ⁻³]	γ_M [cm ³ /s]	β_M [s ⁻¹]	M [cm ⁻³]
1.7×10^{-5}	1.0×10^{-11}	1.6×10^{-11}	300	3.75×10^{15}	1.8×10^{-15}	0.025	2×10^{16}

the TPD-PPV photoconductive host by at least 0.8 eV, i.e., the chromophores do not contribute to carrier trapping.

The value of β_M has been independently determined from double-pulse experiments with defined delay between the subsequent pulses as shown in Fig. 5. As expected, shorter delay times τ reduce the photocurrent of the second pulse, since the number of recombination sites increases with the density of filled traps. For further simulations, we have used the time at which the photocurrent has recovered to 70% of the single-pulse level, yielding $\beta_M = 1/\tau = 0.025 \pm 0.005 \text{ s}^{-1}$. With the ratio of β_M/γ_M as determined above, the value of the deep trapping coefficient is $\gamma_M = (1.8 \pm 0.2) \times 10^{-15} \text{ cm}^3 \text{ s}^{-1}$. Note, that the value of τ compares well with the typical delay time $t_d \approx 50 \text{ s}$ between the gate pulses and the recording of the holograms in PR experiments, for which the effect of preillumination almost vanished.¹⁸ This suggests that deep trap filling is the major process involved in the gating effect.

Compared to the coefficient for recombination and shallow trapping, the deep trapping coefficient is very low. On the other hand, detrapping from deep traps is significant even at RT. One consequence of thermal detrapping is that the degree of trap filling in the steady state is a function of illumination intensity. This, further, implies that the density of ionized sensitizer molecules will be a function of the light intensity. Further note that the intensity dependence became almost linear when the sample was cooled down to a temperature below T_g . This suggests that detrapping from deep traps is assisted by molecular motion. A similar conclusion had been drawn from photocurrent and PR experiments per-

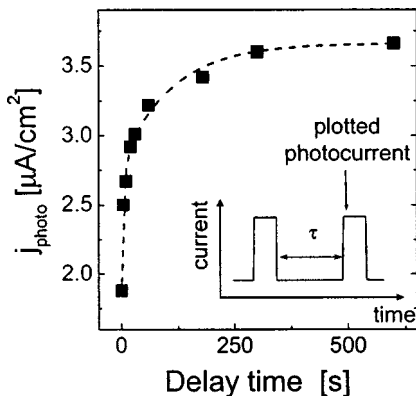


FIG. 5. Dependence of the photocurrent at the end of the second pulse on the delay time between two pulses in double-pulse illumination experiments (pulse length 100 ms). The dashed line is a guide to the eye.

formed on PVK-based composites with glass-transition temperatures below and above room temperature.^{35,36}

Finally, these photoelectrical parameters have been verified by simulating photocurrent transients with different pulse lengths. As an example, simulations of a 140 ms and of a 400 ms pulse are compared to the experimental photocurrent transients in Fig. 3. The agreement is remarkable, having in mind that all parameters have been deduced assuming a constant (time-independent) mobility. However, note that a better agreement to all single pulse measurements was obtained by slightly increasing M to $2.0 \times 10^{16} \text{ cm}^{-3}$. This value was used in the simulation of the PR properties as described below. The complete set of parameters is summarized in Table I.

Simulation of PR properties—0th-order parameters. In order to understand the kinetics of grating formation and the effect of gating in the PR four-wave mixing experiments, the temporal evolution of the density of free charge carriers and of trapped carriers was simulated using Eq. (2) (including both shallow and deep traps), using the writing conditions in the holographic experiment as in Ref. 18 (writing wavelength 830 nm, grating periodicity 3.5 μm , absorption coefficient 5 cm^{-1} , total internal intensity 1.0 W/cm^2 , and applied external field 60 $\text{V}/\mu\text{m}$). For the simulation, a quantum efficiency of $\phi = 0.25$ as measured by xerographic experiments at a field of 60 $\text{V}/\mu\text{m}$ was used. All other photophysical parameters were deduced from the photocurrent experiments as described above, which were performed at a field of around 27 $\text{V}/\mu\text{m}$. We like to point out that according to the large number of investigations on the charge carrier motion in organic materials, the mobility (and with that the trapping coefficients) at the field used in the PR experiment is expected to be larger than at the field used for the photophysical investigations. Also, detrapping might be more efficient at larger fields. We are well aware of these problems, which are mainly due to experimental constraints. Also, for experimental reasons, the wavelength of light utilized in our photophysical studies was different from the wavelength of the writing laser and the light used for the homogeneous preillumination in the PR experiments. Nevertheless, we are of the opinion that the simulations outlined in the following provide a conclusive picture of the processes governing the PR growth in this PR composite.

Without preillumination, the simulated transient of the 0th Fourier component of M^+ as shown in Fig. 6(a) is characterized by a gradual increase extending over several orders of magnitude in time, accompanied by an increase in the density of ionized sensitizer molecules [Fig. 6(c)]. The steady-state is reached after more than 10 s. This behavior closely

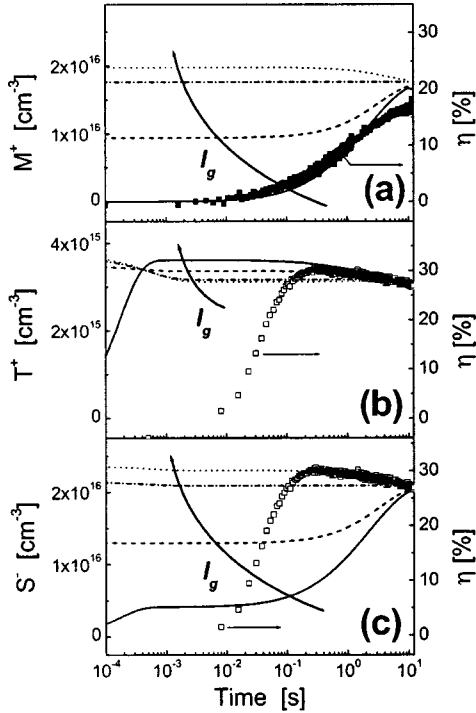


FIG. 6. Simulated transients of the densities (0th order Fourier components) of deep traps (a), shallow traps (b), and ionized sensitizers (c), after gating for 955 ms with an intensity I_g of 0 (solid line), 0.29 (dashed line), 1.45 (dashed-dotted line), and 5.2 (dotted line) W cm^{-2} . The arrows indicate increasing gate intensity. Also shown are experimental PR diffraction scans (squares) without gating (a) or after gating with an intensity of 5.2 W cm^{-2} (b), (c) as taken from Ref. 18.

resembles the PR grating response shown in Fig. 1 of Ref. 18 [also included in Fig. 6(a)]. Even though the diffraction efficiency η is not a linear function of the 0th-order density of filled traps, the rather good agreement between the temporal evolution of M^+ and η suggests that in the absence of preillumination, the PR signal growth is mainly determined by the homogeneous filling of deep traps.

In the second step, the effect of gating has been analyzed by simulating transients immediately following preillumination with various gating intensities I_g (gate pulse length 955 ms, $\lambda = 633 \text{ nm}$, $\alpha = 155 \text{ cm}^{-1}$). Based on the simulations shown in Fig. 6, we conclude that the main effect of gating is the filling of deep traps, accompanied by the creation of a large homogeneous density of ionized sensitizer molecules. Apparently, the PR growth time after intense gating can not be correlated to any specific growth time of the 0th-order parameters. On the other hand, the gradual decay of the PR efficiency for times larger than around 200 ms seems to closely match the decrease in the density of ionized sensitizer molecules [Fig. 6(c)]. Apparently, the density of ionized sensitizer molecules limits the strength of the PR space-charge field in the quasi-steady-state after the initial fast growth.

Simulation of PR properties and space charge field. For illumination with a sinusoidal intensity pattern, the diffraction efficiency η in the holographic degenerate four-wave mixing experiment is given by

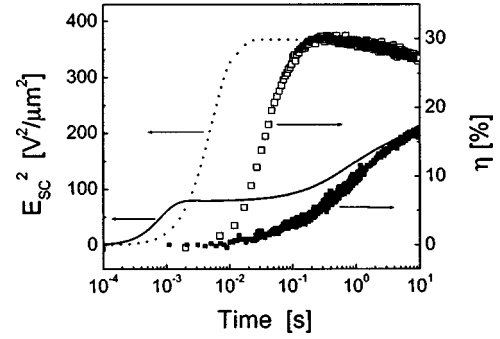


FIG. 7. Square of the space-charge field (first Fourier component) according to simulations without gating (solid line) and immediately after gating with an intensity of 5.2 W cm^{-2} (dotted line), using the parameters listed in Table I. The symbols depict the experimental PR diffraction scans without gating (full squares) or after gating with an intensity of 5.2 W cm^{-2} (open squares) as taken from Ref. 18.

$$\eta = \sin^2 \left(\frac{\pi d \Delta n_1}{\lambda \cos \alpha_i} \right). \quad (7)$$

Here, d is the sample thickness, λ is the wavelength of reading light, α_i is the internal angle of the read beam, and Δn_1 is the first Fourier component of the spatial modulation of the refractive index. Note that Eq. (7) neglects the absorption of light by the PR material. Further, in the limit of *orientational enhancement*, Δn_1 is directly proportional to the first Fourier component of the space charge field $E_{SC,1}$.²⁰ Then, for diffraction efficiencies well below 100%, η should be proportional to the square of $E_{SC,1}$.

The kinetic of $E_{SC,1}$ is determined by the temporal evolution of the first-order Fourier components of the density of holes ρ_1 , ionized sensitizers S_1^- , filled shallow traps T_1^+ , and filled deep traps M_1^+ :

$$E_{SC,1}(t) = \frac{\Lambda}{2\pi} \frac{e}{\epsilon_0 \epsilon} [\rho(t) + T_1^+(t) + M_1^+(t) - S_1^-(t)] \quad (8)$$

with Λ the grating periodicity. The relevant first-order densities as a function of time were calculated on the basis of the coupled system of nonlinear differential equations as published in Refs. 25, 27. In this simulation, the coefficient of the field dependence of the generation efficiency p was set to 0.9 as determined from the results of the xerographic discharge experiments.

Figure 7 compares the predicted transient of $(E_{SC,1})^2$, calculated by taking into account both shallow and deep traps, to the experimentally determined PR growth curves. Without gating, the simulation (solid line) explains the main growth of the diffraction efficiency well (solid symbols). Interestingly, the first sharp step in the predicted transient associated with shallow trap filling does not appear in the experimental holographic growth curve. In fact, a better agreement to the experimental PR data is obtained when neglecting the contribution by shallow traps, while leaving all other parameters unchanged (not shown here). This particular result is not yet understood and requires further investigations. Here, we would like to mention three possible explanations: First, as

outlined above, the photoelectrical investigations have been performed at different conditions (field, wavelength) than the PR experiments. We have no information on the dependence of the shallow and deep trapping coefficients and detrapping rates on the electric field. However note, that if, e.g., shallow detrapping became more rapid at higher electric fields (at the PR writing conditions), the degree of shallow trap occupation and with that the contribution to the space charge field would be smaller than determined from our simulations. Second, based on the rather large trapping coefficient γ_T one might presume that the corresponding sites are charged traps (e.g., ionic impurities, extended dipoles). Those traps are not considered in Schildkraut's model used here. Finally, the initial fast rise of E_{SC} due to shallow trap filling might be "smeared out" by the slower chromophore dynamics as outlined below.

After intense gating (with 5.2 W/cm^2) the simulation predicts a rapid increase of the diffraction efficiency, followed by a plateau and finally a gradual decay. The general shape of the calculated transient compares well with the PR diffraction curve measured after intense gating. However note, that the experimental growth after gating is around a factor of 10 slower than the predicted growth time. Based on recent ellipsometric experiments³⁷ we conclude that the PR response is now limited by the slower orientational dynamics of the chromophores.

The simulation with the parameters listed in Table I yields a maximum strength of the space charge field of around $20 \text{ V}/\mu\text{m}$. This is still well below the projection of the external field on the direction of the grating vector, yielding around $30 \text{ V}/\mu\text{m}$. Unfortunately, the strength of the space charge field in the present system is not known. Kim *et al.* have recently measured the magnitude of the space charge field in a photorefractive composite based on a poly[methyl-3-(9-carbazolyl)propoylsilane] photoconduction matrix sensitized with trinitrofluorone (TNF).³⁸ For an external electric field of $30 \text{ V}/\mu\text{m}$, this material exhibited a diffraction efficiency of 30%. Under these conditions, the space charge field estimated from a comparison of birefringence and PR experiments was around $6 \text{ V}/\mu\text{m}$. Thus, the magnitude of E_{SC} obtained from our simulations seems to be reasonable.

Simulation of PR properties—first-order parameters. At this point the question arises which photophysical processes limit the PR response time. Figures 8(a), 8(b) compare the 0th and first-order Fourier components of the density of ionized sensitizers and filled deep traps. For simplicity, shallow trap filling has not been considered in this simulation. Without gating, the first-order component dominating the rise of the space charge field is the spatial modulation of the density of ionized sensitizer molecules S_1^- . Even after 10 s, the spatial modulation in the ionized sensitizer concentration exceeds that of the first Fourier component of deep trap occupation. Further, the first Fourier component of the density of filled traps is much smaller than the 0th-order component, meaning that the occupation of deep traps is almost constant in space.

According to our simulations, the main process controlling the build-up of the space charge field is the homogenous filling of deep traps $M(t)$. This process concurrently creates

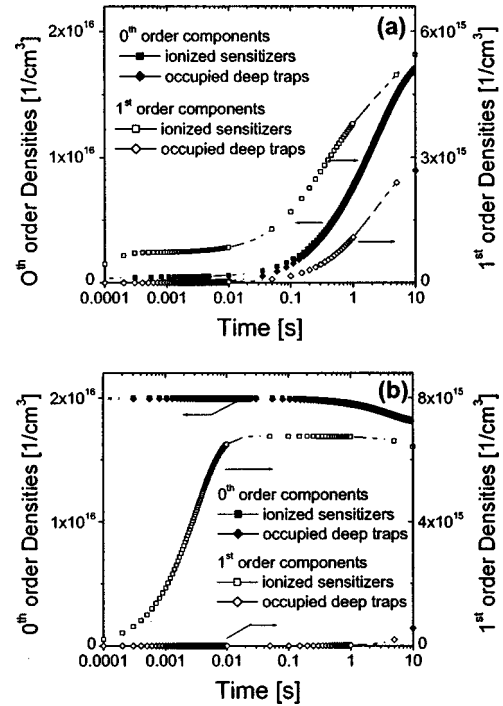


FIG. 8. Simulated transients of the densities (0th and first-order Fourier components) of deep filled traps and ionized sensitizers without (a) and after gating for 955 ms with an intensity I_g of 5.2 W cm^{-2} (b). In this calculation, the density of shallow traps was set to zero.

a large density of negatively charged ionized sensitizer molecules $S(t)$ which finally forms the space charge field [because the filling of shallow traps was neglected and the free carrier density is low, on the order of $10^{14} - 10^{15} \text{ cm}^{-3}$, $M(t)$ is comparable to $S(t)$]. Note that a major prediction of Schildkraut's model is that the steady-state saturation field (the maximum possible space charge field) is linearly proportional to the density of filled traps.^{28,36} Since the kinetics of free holes is fast (compared to the trapping and detrapping) it is meaningful to propose that the density of filled traps also limits the space charge field during the holographic grating growth discussed here. In fact, the simulations in Fig. 8 show that the growth of the space charge field adiabatically follows the homogeneous filling of deep traps.

Assuming that all photogenerated carriers contributed to homogenous trap filling, the time needed to photogenerate the number of carriers necessary to fill all deep traps is approximately determined by

$$\frac{\Delta M}{\Delta t} \approx \frac{M}{\tau_{\text{growth}}} \cong \frac{\phi \alpha I}{h \nu} \quad (9a)$$

resulting in

$$\tau_{\text{growth}} = \frac{h \nu}{\phi \alpha I} M. \quad (9b)$$

Under the experimental PR writing conditions, τ_{growth} is predicted to be few milliseconds, only. This is orders of magnitude faster than the observed PR growth time without preillumination. However, according to our studies, the deep

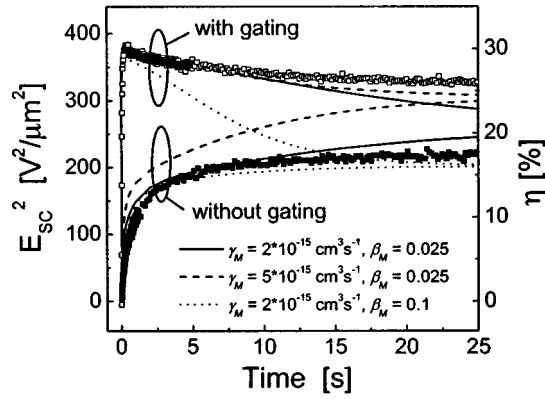


FIG. 9. Square of the space-charge field (first Fourier component) according to simulations without and with intense gating, simulated with different combinations of the deep trapping coefficient γ_M and the detrapping rate β_M . All other parameters are identical to those in Table I.

trapping capture coefficient γ_M is much smaller than the recombination coefficient γ_R . Therefore, most carriers recombine with ionized sensitizer molecules before occupying a deep trap. With γ_M/γ_R around 1/5000, the time to fill all deep traps is estimated to be of the order of seconds, in good agreement to the experimental PR growth time.

Intense gating with homogenous illumination creates a large density of ionized sensitizer molecules and deep traps S_1^- and M_1^+ . The PR dynamics is then determined by the rapid growth of S_1^- , caused by the efficient neutralization of ionized sensitizer molecules in the dark regions by free charge carriers generated in the bright grating areas. In fact, the modulation of the density of trapped charges, as expressed by M_1^+ remains very low throughout the whole simulation. This can be understood by the fact, that after intense gating the degree of deep trap filling is close to saturation. Therefore, the build up of M_1^+ requires detrapping from deep traps, which is a slow process.

Under the assumption that the density of filled traps during writing remains almost constant, the PR speed is entirely governed by the generation of charges and their recombination with ionized sensitizer molecules. The latter process is described by the coefficient γ_R . Compared to the slow deep trap filling governing the charge carrier dynamics in the case without preillumination, the gain in PR growth speed upon gating should, therefore, be related to the large ratio of the coefficients for carrier recombination and trapping. However, note that the initial growth of the signal in the PR experiments considered here is partially determined by the chromophore dynamics, and a quantitative comparison of the growth times with and without gating is not meaningful.

Simulation of PR properties—PR growth time and decay. At this point, we would like to finally comment on the significance of various photophysical parameters in determining the PR growth and decay, without and with gating. Figure 9 shows simulations of $(E_{SC,1})^2$ for different combinations of γ_M and β_M . As outlined above, the main process limiting the growth of the space charge field without gating is the competition between trapping of charges in deep traps and

recombination with ionized sensitizer molecules. Therefore, the initial growth of $(E_{SC,1})^2$ should depend strongly on the chosen value of γ_M . This is clearly expressed by the significant shortening of the PR growth time when increasing γ_M from 2×10^{-15} to 5×10^{-15} $\text{cm}^3 \text{s}^{-1}$. On the other hand, increasing the detrapping coefficient β_M mainly slows down the growth at longer times. Moreover, a larger value of β_M implies a lower degree of deep trap filling in the steady state and, concurrently, a smaller steady-state space charge field.

After intense gating, the predicted PR growth is mainly governed by the generation and recombination kinetics. Consequently, varying the values of γ_M and β_M does not significantly alter the PR growth time. However, increasing β_M strongly affects the gradual decay of the space charge field and, eventually, the steady-state value of $E_{SC,1}$. This decay is due to the fact that the degree of trap filling (and thus of the density of ionized sensitizer molecules) in steady state depends on the light intensity, as mentioned above. Therefore, the values of M_1^+ and S_1^- after intense gating are predicted to exceed the equilibrium densities at the more moderate writing conditions used in the PR experiment. Consequently, both the experimental and simulated PR response after intense gating exhibit a gradual decay due to carrier detrapping from deep traps and recombination with ionized sensitizers. Increasing β_M largely accelerates this decay, while a larger value of γ_M mainly increases the diffraction efficiency in the steady state.

We, finally, would like to note that the agreement between the simulated transients of $(E_{SC,1})^2$, using the photophysical parameters deduced from the photocurrent experiments as described above, and the diffraction efficiencies published earlier¹⁸ is remarkably good for intermediate times between around 100 ms and 10 s. For shorter times, the PR response is apparently limited by the orientational dynamics of the chromophores, which was not taken into account in these simulations. However, the deviation between the simulations and the experimental results for longer times ($t > 10$ s) is yet not understood. We presume that an additional deep trapping level exists, with an even slow detrapping dynamics, which becomes predominately occupied during intense gating. Photophysical experiments covering a larger time range need to be performed to reveal the reason for this discrepancy.

V. CONCLUSIONS

In conclusion, all photophysical parameters relevant to the PR growth in a PPV-based PR composite have been determined from a combination of photocurrent experiments. Based on these parameters, the growth of the space charge field has been simulated, taking into account the effect of preillumination (gating). Without preillumination, the PR growth is governed by the filling of deep traps (Fig. 10). This process concurrently generates the large density of ionized sensitizer molecules, necessary for the build up of the space charge field. The ratio between the coefficients for deep trapping and for the recombination of free charges with ionized sensitizer molecules is identified to be a major factor controlling the PR speed without preillumination. Gating creates a large homogeneous density of ionized sensitizer molecules

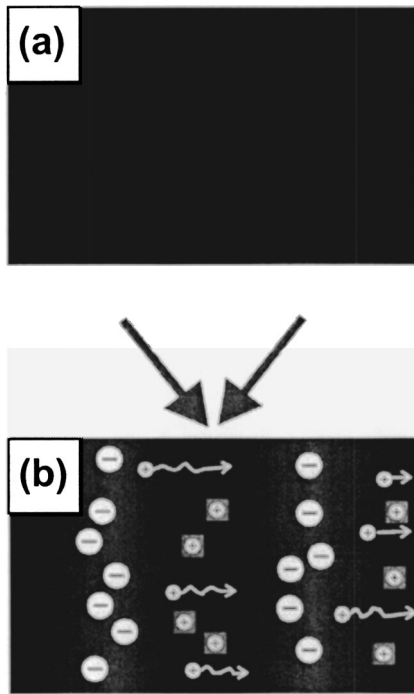


FIG. 10. PR grating formation in the absence of gating. (a) Material does not contain any charges before the PR experiment. (b) PR grating formation is governed by filling of traps and the creation of a spatially modulated ionized acceptor density.

due to deep trap filling (Fig. 11), with the PR growth time now being determined by the kinetics of neutralization of these molecules by free charge carriers. Our simulations can also well explain the long-term decay of the PR diffraction efficiency after intense gating. It is due to the fact that the degree of trap filling in steady-state depends on the illumination intensity. Under the experimental conditions used in Ref. 18 the degree of trap filling and with this the density of ionized sensitizer molecules is larger after intense gating than under the more moderate writing conditions.

We, finally, would like to comment on the applicability of alternative models to determine the PR growth time in this system. According to Yeh,³⁹ there is a fundamental limit for grating formation given by the time required to generate the space-charge density that causes the steady-state space-charge field across one grating period. All other processes, namely, charge transport, charge trapping, and chromophore orientation are assumed to occur instantaneously after the photogeneration of the charge carriers as any finite time involved in these processes can only lengthen the formation time of the grating. Under these assumptions the fundamental limit for the growth time is given by

$$\tau_{\text{SC}} = \frac{2\varepsilon_0\varepsilon E_{\text{SC}}}{e\Lambda} \frac{\hbar\omega}{\alpha\phi I}. \quad (10)$$

With E_{SC} around 20 V/ μm , this limit can be estimated to around 1 ms, well below the measured PR growth time without gating. This discrepancy is expected since Yeh's model neglects the effect of homogenous trap filling and carrier recombination. Consequently, the prediction by Yeh's model

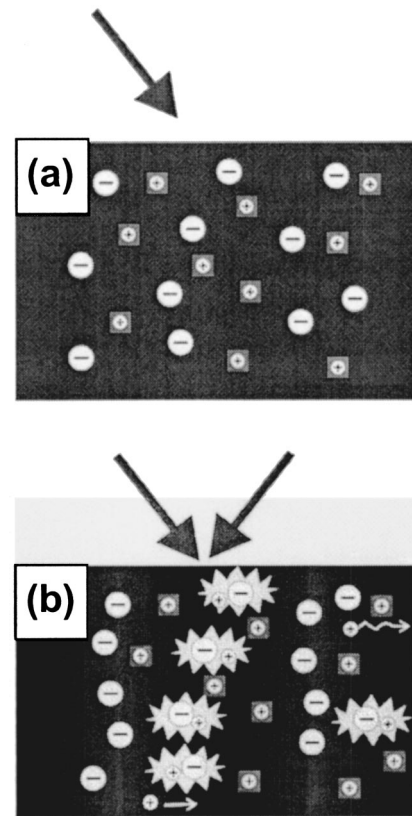


FIG. 11. PR grating formation in the presence of gating. (a) As a result of uniform illumination, the material contains homogeneously distributed charges before the PR experiment. (b) PR grating formation is governed by neutralizing primarily the ionized acceptor density in the dark regions.

is unable to describe the PR growth without gating, but yields a growth time in rather good agreement to our simulation after intense gating.

Alternatively, the simplest version of Kukhtarev²⁶ taking onto account one trapping level has been used to describe PR growth times in organic PR materials. Neglecting contributions by carrier diffusion, the growth of the space charge field is given by

$$\tau_{\text{SC}} = \frac{\varepsilon_0\varepsilon}{e\mu\rho} \left[1 + \left(\frac{2\pi}{\Lambda} L_D \right)^2 \right] \quad (11)$$

with L_D the drift length of free carriers, which is equal to $\mu\tau_D E$. Here, τ_D is the lifetime of carriers, determined by trapping and recombination. If one uses values for ρ and τ_D as calculated under the steady-state PR writing conditions, the magnitude of τ_{SC} is of the order of few milliseconds. Again, this is far below the observed PR growth time. We presume that the failure of this simple model to describe the photorefractive growth kinetics is mainly due to two effects. Assuming only one trapping level, the carrier dynamics in Kukhtarev's model is determined by the photoinduced detrapping of carriers, the drift and the trapping of these carriers. This implies, that the grating dynamics is mainly governed by the crosssection for photoinduced detrapping (which corresponds to the generation coefficient s in the

Schildkraut model) and the coefficient for trapping (which is identical to the trapping coefficient γ_T or γ_M). On the other hand, carrier recombination as described by the coefficient γ_R is not contained in this model. In our case, recombination is fast and a vast fraction of photogenerated carriers recombines before being trapped. Second, Kukhtarev's model is based on the redistribution of a constant number of charge carriers (as supplied by a given density of donor sites). In contrast to that, the initial density of charge carriers (mobile and trapped) in organic PR materials is very low. In fact, since the number of carriers is determined by the competition between generation and recombination, the average density of carriers is a strong function of time (and intensity). We, therefore, presume that the one level Kukhtarev model is not applicable to a vast majority of organic PR composites.

We, finally, want to point out that pronounced effects of preillumination on the PR properties have been reported by others.^{3,21,25,34,40,41} In most of these cases, preillumination

increased the characteristic PR growth time, in contrast to the gating effect observed here. A final explanation of these differences would require a detailed analysis of various PR materials. However, based on our experiments, we propose that the rather low trap density in combination with a large recombination coefficient in our TPD-PPV composite is a major prerequisite for the observed improvement in PR response upon preillumination.

ACKNOWLEDGMENTS

We thank F. Gallego for fruitful discussions. We would also like to acknowledge J.C. Hummelen (University of Groningen, NL) for supplying PCBM. Part of this work was funded by the Volkswagen Foundation and the European Space Agency (Grant No. MAP AO-99-121). Further, O.O. thanks the Killam Trust for financial support.

*Electronic address: neher@rz.uni-potsdam.de

- ¹L. Solymar, D. J. Webb, and A. Grunnet-Jepsen, *The Physics and Applications of Photorefractive Materials* (Clarendon Press, Oxford, 1996).
- ²R. Jones, S. C. W. Hyde, M. J. Lynn, N. P. Barry, J. C. Dainty, W. French, K. M. Kwolek, D. D. Nolte, and M. R. Melloch, *Appl. Phys. Lett.* **69**, 1837 (1996).
- ³B. Kippelen, S. R. Marder, E. Hendrickx, J. L. Maldonado, G. Guillemet, B. L. Volodin, D. D. Steele, Y. Enami, Sandalphon, Y. J. Yao, J. F. Wang, H. Rockel, L. Erskine, and N. Peyghambarian, *Science* **279**, 54 (1998).
- ⁴D. Psaltis, *Science* **298**, 1359 (2002).
- ⁵S. Ducharme, J. C. Scott, R. J. Twieg, and W. E. Moerner, *Phys. Rev. Lett.* **66**, 1846 (1991).
- ⁶K. Meerholz, B. L. Volodin, Sandalphon, B. Kippelen, and N. Peyghambarian, *Nature (London)* **371**, 497 (1994).
- ⁷O. Zobel, M. Eckl, P. Stroehriegl, and D. Haarer, *Adv. Mater. (Weinheim, Ger.)* **7**, 911 (1995).
- ⁸P. M. Lundquist, R. Wortmann, C. Geletnek, R. J. Twieg, M. Jurich, V. Y. Lee, C. R. Moylan, and D. M. Burland, *Science* **274**, 1182 (1996).
- ⁹S. Schlöter, U. Hofmann, P. Stroehriegl, H. W. Schmidt, and D. Haarer, *J. Opt. Soc. Am. B* **15**, 2473 (1998).
- ¹⁰F. Würthner, S. Yao, J. Schilling, R. Wortmann, M. Redi-Abshiro, E. Mecher, F. Gallego-Gomez, and K. Meerholz, *J. Am. Chem. Soc.* **123**, 2810 (2001).
- ¹¹L. Wang, M.-K. Ng, and L. Yu, *Appl. Phys. Lett.* **78**, 700 (2001).
- ¹²C. Hohle, U. Hofmann, S. Schlöter, M. Thelakkat, P. Stroehriegl, D. Haarer, and S. J. Zilker, *J. Mater. Chem.* **9**, 2205 (1999).
- ¹³K. Ogino, S. H. Park, and H. Sato, *Appl. Phys. Lett.* **74**, 3936 (1999).
- ¹⁴O. Ostroverkhova, D. Wright, U. Gubler, W. E. Moerner, M. He, A. Sastre-Santos, and R. J. Twieg, *Adv. Funct. Mater.* **12**, 621 (2002).
- ¹⁵E. Mecher, C. Bräuchle, H. H. Hörhold, J. C. Hummelen, and K. Meerholz, *Phys. Chem. Chem. Phys.* **2**, 1749 (1999).
- ¹⁶U. Hofmann, A. Schreiber, D. Haarer, S. J. Zilker, A. Bacher, D. D. C. Bradley, M. Redecker, M. Inbasekaran, W. W. Wu, and E. P. Woo, *Chem. Phys. Lett.* **311**, 41 (1999).

- ¹⁷W. You, L. Wang, Q. Wang, and L. Yu, *Macromolecules* **35**, 4636 (2002).
- ¹⁸E. Mecher, F. Gallego-Gomez, H. Tillmann, H. H. Hörhold, J. C. Hummelen, and K. Meerholz, *Nature (London)* **418**, 959 (2002).
- ¹⁹H. H. Hörhold, H. Tillmann, D. Raabe, M. Helbig, W. Elfein, A. Bräuer, W. Holzer, and A. Penzkofer, *Proc. SPIE* **4105**, 431 (2001).
- ²⁰W. E. Moerner, S. M. Silence, F. Hache, and G. C. Bjorklund, *J. Opt. Soc. Am. B* **11**, 320 (1994).
- ²¹S. M. Silence, G. C. Bjorklund, and W. E. Moerner, *Opt. Lett.* **19**, 1822 (1994).
- ²²E. Hendrickx, Y. D. Zhang, K. B. Ferrio, J. A. Herlocker, J. Anderson, N. R. Armstrong, E. A. Mash, A. P. Persoons, N. Peyghambarian, and B. Kippelen, *J. Mater. Chem.* **9**, 2251 (1999).
- ²³S. Schlöter, A. Schreiber, M. Grasruck, A. Leopold, M. Kol'chenko, J. Pan, C. Hohle, and P. Stroehriegl, S. J. Zilker, and D. Haarer, *Appl. Phys. B: Lasers Opt.* **68**, 899 (1999).
- ²⁴D. Van Steenwinckel, E. Hendrickx, A. Persoons, K. Van den Broeck, and C. Samyn, *J. Chem. Phys.* **112**, 11030 (2000).
- ²⁵O. Ostroverkhova and K. D. Singer, *J. Appl. Phys.* **92**, 1727 (2002).
- ²⁶N. V. Kukhtarev, V. B. Markov, S. G. Odulov, M. S. Soskin, and V. L. Vinetskii, *Ferroelectrics* **22**, 949 (1979).
- ²⁷J. S. Schildkraut and A. V. Buettner, *J. Appl. Phys.* **72**, 1888 (1992).
- ²⁸J. S. Schildkraut and Y. Cui, *J. Appl. Phys.* **72**, 5055 (1992).
- ²⁹D. Wright, M. A. Diaz-Garcia, J. D. Casperson, M. DeClue, W. E. Moerner, and R. J. Twieg, *Appl. Phys. Lett.* **73**, 1490 (1998).
- ³⁰Y. P. Cui, B. Swedek, N. Cheng, J. Zieba, and P. N. Prasad, *J. Appl. Phys.* **85**, 38 (1999).
- ³¹D. J. Binks and D. P. West, *J. Chem. Phys.* **115**, 6760 (2001).
- ³²T. K. Däubler, A. Meisel, and V. Cimrova (private communication).
- ³³L. Holtmann, *Phys. Status Solidi A* **113**, K89 (1989).
- ³⁴J. A. Herlocker, C. Fuentes-Hernandez, K. B. Ferrio, E. Hendrickx, P. A. Blanche, N. Peyghambarian, B. Kippelen, Y. Zhang, J. F. Wang, and S. R. Marder, *Appl. Phys. Lett.* **77**, 2292 (2000).

- ³⁵R. Bittner, T. K. Däubler, D. Neher, and K. Meerholz, *Adv. Mater. (Weinheim, Ger.)* **11**, 123 (1999).
- ³⁶T. K. Däubler, R. Bittner, K. Meerholz, V. Cimrova, and D. Neher, *Phys. Rev. B* **61**, 13 515 (2000).
- ³⁷F. Gallego and K. Meerholz (unpublished).
- ³⁸W.-J. Joo, N.-J. Kim, H. Chun, I. K. Moon, N. Kim, and C.-H. Oh, *J. Appl. Phys.* **91**, 6471 (2002).
- ³⁹P. Yeh, *Appl. Opt.* **26**, 602 (1987).
- ⁴⁰J. Wolff, S. Schlöter, U. Hofmann, D. Haarer, and S. J. Zilker, *J. Opt. Soc. Am. B* **16**, 1080 (1999).
- ⁴¹D. D. Steele, B. L. Volodin, O. Savina, B. Kippelen, N. Peyghambarian, H. Rockel, and S. R. Marder, *Opt. Lett.* **23**, 153 (1998).